



 Zurich Instruments
Introduction to Lock-in Detection
→ Download the Whitepaper 



Full . Published Online: 18 July 2017 Accepted: July 2017

Lasing in cuprous iodide microwires

Appl. Phys. Lett. 111, 031105 (2017); <https://doi.org/10.1063/1.4990524>

Marcel Wille¹,  Evgeny Krüger¹, Steffen Blaurock², Vitaly Zviagin¹, Rafael Deichsel¹, Gabriele Benndorf¹, Lukas Trefflich¹, Volker Gottschalch², Harald Krautscheid², Rüdiger Schmidt-Grund¹, and  Marius Grundmann¹

View Affiliations

 PDF

ABSTRACT

FULL TEXT

FIGURES

SUPPLEMENTAL

TOOLS

SHARE METRICS

TOPICS

- Excitons
- Crystal structure
- Laser theory
- Semiconductor device fabrication
- Luminescence spectroscopy
- Whispering gallery wave modes
- Cryogenics
- Chemical compounds
- Acoustical properties

ABSTRACT

We report on the observation of lasing in cuprous iodide (CuI) microwires. A vapor-phase transport growth procedure was used to synthesize CuI microwires with low defect concentration. The crystal structure of single microwires was determined to be of zincblende-type. The high optical quality of single microwires is indicated by the observed series of excitonic emission lines as well as by the formation of gain under optical excitation. Lasing of triangular whispering-gallery modes in single microwires is demonstrated for fs- and ns-excitation from cryogenic temperatures up to 200 K. Time-resolved micro-photoluminescence studies reveal the dynamics of the laser process on the time scale of several picoseconds.

Cuprous iodide (CuI) is a wide bandgap semiconductor which has gained interest in the last few years due to its possible application as a transparent conductive material. Specifically, zincblende-type γ -CuI, with direct bandgap energies of 3.115 eV at 4 K and 2.95 eV at 300 K,^{1,2} is of

great interest due to its transparency in the visible spectral range, its intrinsic p-type conductivity, and its high hole-mobility of up to $43 \text{ cm}^2/\text{V s}$.³⁻⁵ Therefore, CuI is well suited as a p-component in optoelectronic devices, i.e., as a collection layer for holes in solar cells and in transparent p-n-heterojunctions.⁶⁻⁸ Micro- and nanostructures of p-type CuI can be complementary building blocks in compact integrated optoelectronic circuits and devices. In particular, the intense photoluminescence (PL) in the near ultraviolet (NUV) range and the high exciton binding energy of 62 meV support the applicability of CuI in optoelectronic devices.⁹ However, the synthesis of CuI micro- and nanostructures and their optical properties are almost unexplored in contrast to other compound semiconductors like zinc oxide (ZnO),¹⁰⁻¹² cadmium sulfide (CdS),^{13,14} gallium nitride (GaN),^{15,16} and gallium arsenide (GaAs).^{17,18}

The aim of this work is to present CuI microstructures as potential candidates for future optoelectronic applications. We applied a vapor-phase transport growth process in order to synthesize high quality microstructures of CuI, characterize their morphology and crystal structure properties, and demonstrate their outstanding ability to act as a laser under optical excitation. The temperature limit of the lasing process in single microwires will be investigated. Using the time-resolved micro-photoluminescence μ -PL technique, the dynamics of the lasing emission of single microwires is investigated in order to reveal information about the underlying decay process.

Cuprous iodide microwires with diameters in the range of $(0.5-50) \mu\text{m}$ and lengths up to several millimeters were synthesized using a vapor-phase transport growth procedure, similar to the process presented by Goto *et al.*¹ The source materials 0.58 g CuI (99.995%, Carl Roth) and 1.22 g iodide (99.5%, Alfa Aesar) were filled into a glass tube (a diameter of 3.5 cm and a length of 25 cm). After cooling the mixed solid powders in liquid nitrogen, the glass tube was evacuated to a pressure of $<10^{-3}$ mbar and subsequently sealed. The growth of CuI microwires took place in a three-zone-furnace with a linear temperature profile between 250 °C and 450 °C. The glass tube was kept in the furnace for 4 weeks at an inclination angle of 10° . The largest amount of microwires was found in the central part of the glass tube. Scanning electron microscopy (SEM) was used to examine the morphology and structural properties of single microwires. X-ray diffraction (XRD) patterns were recorded in order to study the crystal structure of CuI microwires. The chemical composition was examined using energy dispersive X-ray spectroscopy (EDX) equipped in

the SEM system. For subsequent spatially resolved PL investigations, the microwires were transferred onto a clean SiO₂/Si substrate using an acupuncture needle. The thermally grown low refractive index SiO₂-layer (thickness of 1.5 μm, $n_{\text{SiO}_2} = 1.47$ at 3.0 eV photon energy) causes a reduction of leakage of the electromagnetic field into the substrate.¹⁴ The substrate with the microwire samples was mounted either in a helium bath cryostat with a sample temperature of 2 K or in a helium flow cryostat in order to perform temperature dependent measurements in the range of (14–300) K. A frequency doubled titanium-sapphire (Ti:Sa) laser ($\lambda_{\text{ex}} = 364$ nm, $t_{\text{pulse}} = 200$ fs, and $f_{\text{rep}} = 76$ MHz) was used as an excitation laser for time-integrated as well as time-resolved PL measurements at 2 K and at low excitation densities. The PL was spectrally dispersed by a spectrometer (focal length of 320 mm, 2400 lines/mm) and guided either to a CCD camera (spectral resolution of 0.3 meV) or to a time-correlated single-photon counting setup with a time resolution of 20 ps (details can be found in Ref. 19). For μ -PL measurements at high excitation densities, a frequency mixed Nd:YAG laser ($\lambda_{\text{ex}} = 355$ nm, $f_{\text{rep}} = 100$ Hz, and $t_{\text{pulse}} = 10$ ns) and the fs-pulsed Ti:Sa laser were used. The laser beam was focused by a 50× microscope objective to a spot size of (10–50) μm² for the non-resonant excitation of single microwires. The PL was collected by the same objective, dispersed by a spectrometer and guided either to a CCD camera (spectral resolution of 0.5 meV) or to a streak camera (Hamamatsu C5680) with a time resolution of 2 ps. A variable attenuator was used to adjust the excitation density. The laser power was measured using a calibrated Si diode power meter.

The analysis of the morphology of zincblende-type CuI indicates different growth kinetics, as already shown by Grundmann *et al.*²⁰ It was found from SEM investigations that larger microwires often exhibit a belt-like shape (see Fig. S1 in the [supplementary material](#)). However, smaller microwires crystallize symmetrically to the wire axis and exhibit a rounded triangular cross-section. Figures 1(a) and 1(b) show the SEM images of an exemplary CuI microwire with triangular shape. This microwire has a length of 49 μm and an approximate diameter of 4.0 μm. The microwire surfaces are smooth and free of any apparent defects. The chemical composition of several single microwires with different cross-section dimensions was analyzed using the EDX technique. The EDX spectra (see Fig. S2 in the [supplementary material](#)) reveal the stoichiometric ratio Cu/I \approx 1/1. X-ray diffraction measurements (see Fig. S3 in the [supplementary material](#)) prove that the microwires crystallize

in the zincblende structure (γ -CuI). XRD patterns, taken from a side facet of a belt-like microwire, yield the [111]-orientation of zincblende CuI. However, a detailed analysis of the different growth kinetics of the presented microwires is still pending.

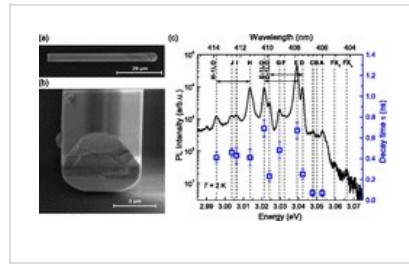


FIG. 1.

(a) SEM image of a CuI microwire with a length of 49 μm and a diameter of around 4.0 μm . The high resolution SEM image in (b) was taken at a tilt

angle of 45° and reveals a rounded triangular microwire cross-section. (c) The PL spectra (Ti:Sa, $P_{\text{ex}} = 0.3 \text{ nJ/cm}^2$) at a temperature of 2 K exhibit a series of excitonic emission lines. The energies of the labeled transitions are listed in Table I. Time-resolved PL measurements reveal the respective decay times [blue squares in (d)]. Black arrows represent the energy spacing between an emission line and its LO-phonon replica.

↓ PPT | High-resolution

The PL measurements at low excitation density and 2 K substrate temperature were performed on six microwires; therefore, both belt-like and triangular microwires have been investigated. All microwires exhibit similar emission characteristics; however, the PL signal from triangular microwires is less intense because of the smaller volume. Figure 1(c) shows the PL spectra from a belt-like microwire with a length of 865 μm and cross-section dimensions of 17.9 $\mu\text{m} \times 3.8 \mu\text{m}$ (SEM image is shown in Fig. S1 in the [supplementary material](#)) for an excitation density of $P_{\text{ex}} = 0.3 \text{ nJ/cm}^2$ (1.7 kW/cm^2). The observed excitonic transitions are listed in Table I. The distinct peaks at 3.0662 eV and 3.0596 eV can be assigned to the longitudinal free exciton (FX_L) and the transverse free exciton (FX_T), respectively.^{9,21–23} The energy spacing of 6.6 meV fits quite well to the known L-T-splitting energy in CuI.^{23,24} A direct comparison of the transitions at lower energies with literature data is rather difficult due to strongly varying emission characteristics depending on the growth conditions, strain, and electronic and structural defects.^{25,26} A strong emission in the energy range of the most intense lines D and E was also observed by Vereshchagin *et al.*²⁷ and was assigned to shallow neutral acceptor transitions. Sauder and Certier²⁸ ascribed an intense line in the energy range of the observed emission line H to the emission

of excitons bound to neutral acceptors originating from surface near copper vacancies. Note that the emission energy of the bound excitons changes slightly along the microwire axis (maximum deviation of 6 meV for the line H). This might be due to the irregular defect incorporation during the growth process. The decay characteristics of the individual excitonic emission lines were investigated with a time-correlated single-photon counting setup. The characteristic decay times were evaluated by modeling a mono-exponential decay. In the energy range close to the free excitons, the emission decays with a decay time of around (64 ± 30) ps. With increasing binding energy of the bound excitons, the decay time increases and reaches a value of (680 ± 80) ps for the emission line E. The assigned phonon replica ($E_{LO} \approx 18.0$ meV) of the transitions D, E, and H showed similar dynamics to the respective zero-phonon-lines.¹ In contrast, the emission lines I and J, which might be the 2-LO-phonon replica of the lines D and E, exhibit significantly shorter decay times compared to the respective zero-phonon-lines. This could be artificially caused by the spectral overlap with the intense adjacent transitions H and H-1LO which have a decay time of approximately 410 ps. Hence, the origin of the lines I and J remains unclear.



TABLE I. Emission lines and the respective decay times obtained from a CuI microwire at 2 K.

Excitation density dependent μ -PL measurements were performed on microwires with triangular cross-section. Their smaller dimensions lead to a less pronounced absorptive lasing mode suppression, which is induced by the spatially inhomogeneous excitation and the limited carrier diffusion length.¹² Figure 2(a) shows the temperature dependent μ -PL spectra from the microwire shown in Fig. 1, at low (dashed lines) and high (solid lines) excitation densities using the ns-pulsed Nd:YAG laser. For low excitation density at 14 K, the emission from bound excitons (C-, D-, E-, and H-bands) and their LO-phonon replica can be observed. Furthermore, an additional band appears in the energy range of (3.025–3.031) eV. This band most likely originates from inelastic exciton-exciton scattering (P-band), where the radiatively decaying exciton emits a photon and scatters another exciton into a higher excited state.²⁹ Tanaka and Nakayama³⁰ demonstrated the P-band-correlated optical gain of ~ 400 cm⁻¹ in CuI thin films using the stripe length technique and studied the accompanied stimulated emission. With increasing excitation density, bound exciton related emission saturates. At a certain excitation

density, narrow emission lines appear in the spectral vicinity of the P-band emission. These narrow lines were observed up to a temperature of 200 K for an excitation density of 460 kW/cm^2 [solid lines in 2(a)]. Above this critical temperature, a dramatic decrease in PL intensity was observed. With increasing sample temperature, the P-band becomes less pronounced at low excitation density and vanishes at around 150 K. This might be caused by the ineffective scattering of excitons at higher temperatures. As a consequence, P-band correlated gain and thus the lasing process break down above a critical temperature. The excitation density dependent μ -PL spectra at 200 K, using the fs-pulsed Ti:Sa laser as the excitation source, are shown in Fig. 2(b). They clearly demonstrate the transition from broad spontaneous emission to stimulated emission from narrow modes. In order to prove lasing action of single microwires, the input-output characteristic was analyzed. Figure 2(c) depicts the integrated μ -PL intensity of a lasing mode as a function of the excitation density. The double-logarithmic plot shows a distinct S-shaped characteristic which represents the threshold behavior of the lasing transition. The lasing threshold density $P_{\text{th}} = 300 \mu\text{J/cm}^2$ was determined by modeling the excitation density dependent integrated μ -PL intensity with a multimodal laser approach.³¹ Below P_{th} , the emission intensity increases linearly with the excitation density. In the threshold regime, the slope becomes strongly nonlinear and tends to saturate in the lasing regime. This observation clearly demonstrates lasing in the investigated microwire. Overcoming a further threshold at around $650 \mu\text{J/cm}^2$, the mode intensity declines reversibly due to the enhancement of modes at lower energies [data shown in dark green in Figs. 2(b) and 2(c)]. Note that we confirmed lasing at temperatures up to 200 K for several individual microwires with triangular cross-section.

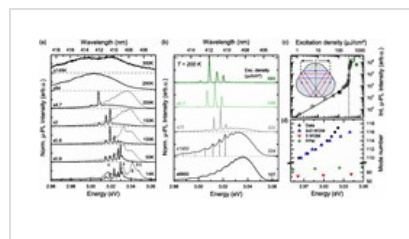


FIG. 2.

(a) The μ -PL spectra (Nd:YAG, $P_{\text{ex}} = 460 \text{ kW/cm}^2$) from the triangular microwire using ns-excitation reveal a stable lasing process for temperatures

up to 200 K (solid lines). The respective μ -PL spectra below the lasing threshold ($P_{\text{ex}} \sim 0.1P_{\text{th}}$) are depicted as dashed lines. (b) Excitation density dependent μ -PL spectra (Ti:Sa) from the same microwire using fs-excitation reveal a transition from broad spontaneous emission to emission from narrow modes at 200 K. (c) Double-logarithmic plot of the integrated μ -PL intensity of a lasing mode in dependence on the excitation density indicates a lasing threshold

density $P_{th} \approx 300 \mu\text{J}/\text{cm}^2$. The filled squares correspond to the spectra in (b). The inset in (c) sketches different types of possible resonant modes in the triangular microwire geometry [green: Fabry-Perót modes (FPM) and red and blue: first- and second-order triangular whispering-gallery modes (3-WGM, 2×3 -WGM), respectively]. (d) The experimentally deduced mode positions at 200 K (black squares) compared to theoretical mode positions of FPM (green circles), 3-WGM (red triangles), and 2×3 -WGM (blue triangles) for a CuI microwire with a dimension $l = 3.16 \mu\text{m}$ and a refractive index $n = (2.472 \dots 2.550)$ obtained from spectroscopic ellipsometry measurements on a CuI thin film (see Fig. S4 in the [supplementary material](#)).

↓ PPT | [High-resolution](#)

The spectral mode positions were analyzed in order to deduce the dominant mode type of the microwire cavity. Figure 2(d) depicts the experimentally observed mode positions at 200 K. The data were extracted slightly below P_{th} [dark gray curve in Fig. 2(b)]. The mode spacing increases significantly from around 4.8 meV to around 13.6 meV with decreasing mode energy. For the triangular microwire, we assume three different types of lateral lasing modes: Fabry-Pérot modes (FPM) and triangular whispering-gallery modes (WGM) of first- (3-WGM) and second order (2×3 -WGM), as depicted in the inset of Fig. 2(c). A Fabry-Pérot cavity model (green) does not fit the mode positions. A plane wave model for TE-polarized WGM in triangular cavities (analogous to hexagonal cavities by Wiersig³²) predicts

$$E = \frac{hc}{nL} \left(N + \frac{m}{\pi} \arctan \left(n \sqrt{\frac{n^2 - 4}{3}} \right) \right). \quad (1)$$

Here, h is Planck's constant, c is the vacuum speed of light, n is the energy dependent refractive index, L is the resonator length, N is the interference order, and m is the number of total internal reflections. For first- and second-order triangular modes, we find $L_3 \approx 3l$, $m_3 = 3$ and $L_{2 \times 3} \approx 6l$, $m_{2 \times 3} = 6$, respectively. From spectroscopic ellipsometry measurements of a CuI thin film (see Fig. S4 in the [supplementary material](#)), we obtained the refractive index $n = (2.472 \dots 2.550)$ in the spectral range of the observed lasing emission. The predicted mode positions for 2×3 -WGM fit the experimentally determined values quite well, as can be seen in Fig. 2(d). Here, a microwire dimension $l = 3.16 \mu\text{m}$ was used, which corresponds well to the SEM data. These findings

indicate strongly that the triangular microwire acts as a whispering-gallery type resonator for second-order triangular modes. The slight deviations in the vicinity of the exciton resonance might arise from the differences between the refractive indices of the measured thin film and the microwires.

The dynamics of the microwire lasers was investigated in the temperature range of (14–200) K using a streak camera. Figure 3(a) shows the time-resolved spectra of the lasing emission from the microwire for an excitation density of $2.5P_{th}$ at 14 K. The transient of the most intense lasing mode is shown in Fig. 3(b). Modeling the decay of this lasing mode with a mono-exponential function yields the characteristic decay time $\tau_L = (6.7 \pm 2.0)$ ps in the lasing regime. Upon variation of the excitation density from P_{th} to $2.5P_{th}$, τ_L fluctuates statistically in the range of (3.5–8.5) ps independent of the sample temperature. The small decay time τ_L reflects the ultrafast recombination after the strong excitation pulse. Ichida *et al.*³³ studied the optical gain in CuI thin films and determined a similar decay time of 8 ps under high optical excitation. They ascribed this fast recombination process to an effective scattering of excitons (P-band). The emission energy and the slight red-shift for higher excitation densities agree with the results found here. However, the formation of an electron-hole-plasma would also cause sufficiently high gain to overcome the resonator losses, evoke a red-shift with increasing excitation density, and cause similar characteristic decay times in the lasing regime, like in other semiconductors.³⁴ Hence, further investigations are necessary to understand the gain mechanism of the observed lasing in CuI microwires.

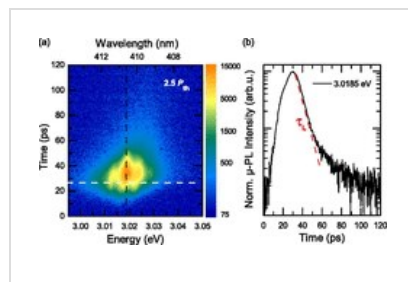


FIG. 3.

(a) Time-resolved μ -PL spectra from the triangular microwire at 14 K (Ti:Sa, $2.5 P_{th}$). Note the logarithmic color scale. The dashed white line indicates the impingement of the excitation

laser pulse. (b) Normalized transient of the most intense lasing mode extracted at the energy 3.0185 eV (indicated by the black dashed line in (a)) exhibits the characteristic decay time $\tau_L = (6.7 \pm 2.0)$ ps.

[↓ PPT](#) | [High-resolution](#)

In summary, we have synthesized [111]-oriented zincblende-type CuI

microwires by applying a vapor-phase transport growth procedure. Their outstanding optical properties constitute in a series of excitonic emission lines at low excitation density conditions. Time-resolved PL measurements at 2 K revealed the decay times of individual free and bound excitons. We demonstrated the observation of lasing of second-order triangular modes in CuI microwires with triangular cross-section for ns- and fs-pulsed laser excitation with threshold densities of 400 kW/cm² and 300 μJ/cm² (1.5 GW/cm²), respectively. We showed that the lasing process is stable up to a temperature of 200 K. The lasing emission was observed in the energy range where the exciton-exciton scattering related P-band is expected. The dynamics of the microwire lasing emission was investigated for different temperatures as well as excitation densities and revealed a characteristic decay time $\tau_L = (3.5\text{--}8.5)$ ps.

See [supplementary material](#), which contains the experimental results of the EDX, XRD, and ellipsometry measurements as well as a description of the respective techniques.

This work was supported by the Deutsche Forschungsgemeinschaft within Gr 1011/26-1 and through FOR1616, by the “Leipzig Graduate School of Natural Sciences – BuildMoNa” and by Universität Leipzig in the framework of research profile area “Complex Matter.” We thank M. Kneiß, C. Sturm, and B. Rheinländer for valuable discussions and C. Yang for the growth of CuI thin films for ellipsometry measurements.

REFERENCES

1. T. Goto, T. Takahashi, and M. Ueta, *J. Phys. Soc. Jpn.* **24**, 314 (1968).
<https://doi.org/10.1143/JPSJ.24.314>,
[Google Scholar](#), [Crossref](#), [CAS](#)

2. S. Ves, D. Glötzel, M. Cardona, and H. Overhof, *Phys. Rev. B* **24**, 3073 (1981).
<https://doi.org/10.1103/PhysRevB.24.3073>,
[Google Scholar](#), [Crossref](#), [CAS](#)

3. J. Wang, J. Li, and S.-S. Li, *J. Appl. Phys.* **110**, 054907 (2011).
<https://doi.org/10.1063/1.3633220>,

4. C. Yang, M. Kneiß, M. Lorenz, and M. Grundmann, Proc. Natl. Acad. Sci. U.S.A. **113**, 12929 (2016).
<https://doi.org/10.1073/pnas.1613643113>,
[Google Scholar](#), [Crossref](#), [CAS](#)

5. D. Chen, Y. Wang, Z. Lin, J. Huang, X. Chen, D. Pan, and F. Huang, Cryst. Growth Des. **10**, 2057 (2010).
<https://doi.org/10.1021/cg100270d>,
[Google Scholar](#), [Crossref](#), [CAS](#)

6. J. A. Christians, R. C. Fung, and P. V. Kamat, J. Am. Chem. Soc. **136**, 758 (2013).
<https://doi.org/10.1021/ja411014k>,
[Google Scholar](#), [Crossref](#)

7. F.-L. Schein, H. von Wenckstern, and M. Grundmann, Appl. Phys. Lett. **102**, 092109 (2013). <https://doi.org/10.1063/1.4794532>,
[Google Scholar](#), [Scitation](#)

8. C. Yang, M. Kneiß, F.-L. Schein, M. Lorenz, and M. Grundmann, Sci. Rep. **6**, 21937 (2016)
<https://doi.org/10.1038/srep21937>.
[Google Scholar](#), [Crossref](#), [CAS](#)

9. S. Nikitine, Philos. Mag. **4**, 1 (1959).
<https://doi.org/10.1080/14786435908238225>
, [Google Scholar](#), [Crossref](#), [CAS](#)

10. M. Huang, S. Mao, H. Feick, H. Yan, Y. Wu, H. Kind, E. Weber, R. Russo, and P. Yang, Science **292**, 1897 (2001).
<https://doi.org/10.1126/science.1060367>,
[Google Scholar](#), [Crossref](#), [CAS](#)

11. C. Czekalla, T. Nobis, A. Rahm, B. Cao, J.

Zúñiga-Pérez, C. Sturm, R. Schmidt-Grund, M. Lorenz, and M. Grundmann, *Phys. Status Solidi B* **247**, 1282 (2010).

<https://doi.org/10.1002/pssb.200945527>,

[Google Scholar](#), [Crossref](#), [CAS](#)

12. M. Wille, T. Michalsky, E. Krüger, M. Grundmann, and R. Schmidt-Grund, *Appl. Phys. Lett.* **109**, 061102 (2016).

<https://doi.org/10.1063/1.4960660>,

[Google Scholar](#), [Scitation](#)

13. R. Agarwal, C. Barrelet, and C. Lieber, *Nano Lett.* **5**, 917 (2005).

<https://doi.org/10.1021/nl050440u>,

[Google Scholar](#), [Crossref](#), [CAS](#)

14. R. Röder, M. Wille, S. Geburt, J. Rensberg, M. Zhang, J. Lu, F. Capasso, R. Buschlinger, U. Peschel, and C. Ronning, *Nano Lett.* **13**, 3602 (2013). <https://doi.org/10.1021/nl401355b>,

[Google Scholar](#), [Crossref](#)

15. J. Johnson, H.-J. Choi, K. Knutsen, R. Schaller, P. Yang, and R. Saykally, *Nat. Mater.* **1**, 106 (2002). <https://doi.org/10.1038/nmat728>,

[Google Scholar](#), [Crossref](#), [CAS](#)

16. C. Tessarek, R. Röder, T. Michalsky, S. Geburt, H. Franke, R. Schmidt-Grund, M. Heilmann, B. Hoffmann, C. Ronning, M. Grundmann *et al.*, *ACS Photonics* **1**, 990 (2014). <https://doi.org/10.1021/ph500220v>,

[Google Scholar](#), [Crossref](#), [CAS](#)

17. X. Duan, J. Wang, and C. M. Lieber, *Appl. Phys. Lett.* **76**, 1116 (2000).

<https://doi.org/10.1063/1.125956>,

[Google Scholar](#), [Scitation](#), [CAS](#)

18. D. Saxena, S. Mokkapati, P. Parkinson, N. Jiang, Q. Gao, H. Tan, and C. Jagadish, *Nat. Photonics* **7**, 963 (2013).
<https://doi.org/10.1038/nphoton.2013.303>,
[Google Scholar](#), [Crossref](#), [CAS](#)
-
19. A. Müller, M. Stölzel, C. Dietrich, G. Benndorf, M. Lorenz, and M. Grundmann, *J. Appl. Phys.* **107**, 013704 (2010).
<https://doi.org/10.1063/1.3270431>,
[Google Scholar](#), [Scitation](#)
-
20. M. Grundmann, F.-L. Schein, M. Lorenz, T. Böntgen, J. Lenzner, and H. von Wenckstern, *Phys. Status Solidi A* **210**, 1671 (2013).
<https://doi.org/10.1002/pssa.201370056>,
[Google Scholar](#), [Crossref](#), [CAS](#)
-
21. V. Nikitenko, S. Stoyukhin, V. Popolitov, and Y. M. Minizon, *J. Appl. Spectrosc.* **34**, 410 (1981). <https://doi.org/10.1007/BF00614221>,
[Google Scholar](#), [Crossref](#)
-
22. T. Sauder, A. Daunois, J. Deiss, and J. Merle, *Solid State Commun.* **51**, 323 (1984).
[https://doi.org/10.1016/0038-1098\(84\)90697-5](https://doi.org/10.1016/0038-1098(84)90697-5),
[Google Scholar](#), [Crossref](#), [CAS](#)
-
23. J. Serrano, C. Schweitzer, C. Lin, K. Reimann, M. Cardona, and D. Fröhlich, *Phys. Rev. B* **65**, 125110 (2002).
<https://doi.org/10.1103/PhysRevB.65.125110>,
[Google Scholar](#), [Crossref](#)
-
24. S. Suga, K. Cho, Y. Niji, J. Merle, and T. Sauder, *Phys. Rev. B* **22**, 4931 (1980).
<https://doi.org/10.1103/PhysRevB.22.4931>,
[Google Scholar](#), [Crossref](#), [CAS](#)
-

25. P. Gao, M. Gu, X. Liu, Y.-Q. Zheng, and E. Shi, *Optik* **125**, 1007 (2014).

<https://doi.org/10.1016/j.ijleo.2013.07.112>,

[Google Scholar](#), [Crossref](#), [CAS](#)

26. G. Lin, F. Zhao, Y. Zhao, D. Zhang, L. Yang, X. Xue, X. Wang, C. Qu, Q. Li, and L. Zhang, *Materials* **9**, 990 (2016).

<https://doi.org/10.3390/ma9120990>,

[Google Scholar](#), [Crossref](#)

27. I. Vereshchagin, V. Nikitenko, and S. Stoyukhin, *J. Lumin.* **29**, 215 (1984).

[https://doi.org/10.1016/S0022-2313\(84\)90008-7](https://doi.org/10.1016/S0022-2313(84)90008-7)

, [Google Scholar](#), [Crossref](#), [CAS](#)

28. T. Sauder and M. Certier, *Phys. Lett. A* **101**, 55 (1984).

[https://doi.org/10.1016/0375-9601\(84\)90092-6](https://doi.org/10.1016/0375-9601(84)90092-6)

, [Google Scholar](#), [Crossref](#)

29. C. Klingshirn and H. Haug, *Phys. Rep.* **70**, 315 (1981).

[https://doi.org/10.1016/0370-1573\(81\)90190-3](https://doi.org/10.1016/0370-1573(81)90190-3)

, [Google Scholar](#), [Crossref](#), [CAS](#)

30. I. Tanaka and M. Nakayama, *J. Appl. Phys.* **92**, 3511 (2002).

<https://doi.org/10.1063/1.1502205>,

[Google Scholar](#), [Scitation](#), [CAS](#)

31. L. Casperson, *J. Appl. Phys.* **46**, 5194 (1975).

<https://doi.org/10.1063/1.321311>,

[Google Scholar](#), [Scitation](#), [CAS](#)

32. J. Wiersig, *Phys. Rev. A* **67**, 023807 (2003).

<https://doi.org/10.1103/PhysRevA.67.023807>,

33. H. Ichida, Y. Kanematsu, T. Shimomura, K. Mizoguchi, D. Kim, and M. Nakayama, Phys. Rev. B **72**, 045210 (2005).

<https://doi.org/10.1103/PhysRevB.72.045210>,

[Google Scholar](#), [Crossref](#)

34. K. Bohnert, G. Schmieder, and C. Klingshirn, Phys. Status Solidi B **98**, 175 (1980).

<https://doi.org/10.1002/pssb.2220980117>,

[Google Scholar](#), [Crossref](#), [CAS](#)

Published by AIP Publishing.

HIDEN
ANALYTICAL

Mass
Spectrometers
for
Surface
Analysis

[Click Here](#)

HiddenAnalytical.com

AUTHOR

ABOUT

PRIVACY POLICY

LIBRARIAN

CONTACT

TERMS OF USE

ADVERTISER

HELP

FOLLOW AIP PUBLISHING:



This website uses cookies to ensure the best user experience. [Learn more](#)

Got it!